Analysis of the Fenton–Karma model through an approximation by a one-dimensional map

E. G. Tolkacheva
Department of Physics and Center for Nonlinear and Complex Systems, Duke University, Durham, North Carolina 27708

D. G. Schaeffer
Department of Mathematics and Center for Nonlinear and Complex Systems, Duke University, Durham, North Carolina 27708

D. J. Gauthier
Department of Physics, Department of Biomedical Engineering, and Center for Nonlinear and Complex Systems, Duke University, Durham, North Carolina 27708

C. C. Mitchell
Department of Mathematics, Duke University, Durham, North Carolina 27708

(Received 30 April 2002; accepted 23 August 2002; published 29 October 2002)

The Fenton–Karma model is a simplification of complex ionic models of cardiac membrane that reproduces quantitatively many of the characteristics of heart cells; its behavior is simple enough to be understood analytically. In this paper, a map is derived that approximates the response of the Fenton–Karma model to stimulation in zero spatial dimensions. This map contains some amount of memory, describing the action potential duration as a function of the previous diastolic interval *and* the previous action potential duration. Results obtained from iteration of the map and numerical simulations of the Fenton–Karma model are in good agreement. In particular, the iterated map admits different types of solutions corresponding to various dynamical behavior of the cardiac cell, such as 1:1 and 2:1 patterns. © *2002 American Institute of Physics.* [DOI: 10.1063/1.1515170]

Developing mathematical models that represent the dynamics of a cardiac cell is important for understanding life-threatening diseases such as ventricular fibrillation (often the cause of sudden cardiac death) and developing therapies for cardiac disease. One approach for modeling the electrical activity of a cardiac cell is to incorporate all known details, such as changes in ionic concentrations and mechanisms that regulate the in- and efflux of ions through the cell membrane. Unfortunately, such detailed models often defy simple mathematical analysis. Another approach is to devise simplified mathematical models that incorporate what is hoped to be the essential elements of the more complex ionic-based models. One such model of the cardiac membrane is a set of ordinary differential equations that keeps track of the transmembrane voltage and three ionic currents as proposed recently by Fenton and Karma. We have investigated the Fenton–Karma model using a multiscale analysis technique and find that the cell dynamics can be represented under some conditions by a mathematical mapping that relates the current duration of an action potential to the duration of the preceding one and the preceding diastolic interval. Such an analysis should simplify fitting the model to experimental observations and lead to new predictions.

I. INTRODUCTION

Control of complexity in the heart has been the focus of recent research on spatiotemporal complexity in dynamical systems. In order to optimally control the electrical activity of the heart, it is important to understand its dynamical properties. Ionic models describing the electrical activity of the cardiac cell[1–4] are becoming more and more complex. These models characterize the total current flowing through the membrane by combining various membrane currents obtained in voltage-clamp or patch-clamp experiments. For instance, the model described in Ref. 4, which is based on data from mammalian cardiac cells, consists of 12 currents. The complexity of these models makes it difficult to analyze results and to carry out two- and three-dimensional simulations.

There have been several simple nonionic models proposed to represent cardiac tissue (see, for instance, Refs. 5 and 6), but they do not encompass as many aspects of heart dynamics as do the ionic models. The Fenton–Karma (FK) ionic model[7] is a simplification of the Luo–Rudy I (LR1) model of the cardiac membrane[2] that reproduces quantitatively much of the behavior of the full model. The FK model contains three currents, loosely corresponding to sodium, calcium, and potassium. It is complex enough to exhibit many of the characteristics of heart cells, yet is simple enough that much of its behavior can be understood analytically. Analytical insight is important because, for example, it will guide the selection of the many parameters that need to be adjusted in fitting the model to experiments.

One tool for analyzing results obtained from numerical simulations of ionic models or experiments is to use a finite-difference equation or map.[8] This allows a reduced description of the trajectory of the ordinary differential equation

(ODE) by a single number, the action potential duration (APD). Usually, following the pioneering conceptual foundation put forth by Mines,[9] maps describing localized cardiac dynamics relate the APD to the previous diastolic interval (DI) through a restitution function,

$$\mathrm{APD}_{n+1}=F(\mathrm{DI}_n). \tag{1}$$

Such a simple mapping model was proposed in Ref. 10 and later generalized in Refs. 11–14. [A restitution mapping of the form (1) was obtained in Ref. 14 in a similar spirit; see also Ref. 15 for a more detailed treatment.]

A more complex model, which includes a phenomenological memory term describing the long-term evolution of tissue properties, was developed and analyzed by Otani and Gilmour[16] to describe a series of experiments on paced Purkinje fibers.[17] Their model differs from previous models in that the APD is a function of two variables,

$$\mathrm{APD}_{n+1}=G(\mathrm{DI}_n,\mathrm{APD}_n). \tag{2}$$

[In one sense the memory in (2) is a not-at-all long term: APD_{n+1} depends on no information prior to the previous action potential. However, under periodic stimulation (see Sec. III), this mapping, or even (1), can exhibit a long-term-memory effect: if the basic cycle length is changed, it may happen that many stimuli are required before the system settles into a new steady-state.]

In this paper we apply multiscale analysis to the FK ionic model to derive a restitution mapping with memory of the form proposed by Otani and Gilmour given by Eq. (2). Thus, this paper strengthens the foundation of their model, which had been purely empirical.

The paper is organized in the following way. In Sec. II we introduce the FK model describing the cardiac cell response to periodic stimulation in zero spatial dimensions (a set of coupled ODE's). In Sec. III we derive a simplified map and show that results obtained from numerical simulations of the FK model and from iteration of the map are in reasonable agreement. In Sec. IV we make three refinements of the map in order to achieve better agreement between these results. Section V presents conclusions.

II. THE FENTON–KARMA MODEL

The Fenton–Karma ionic model[7] contains three variables: the transmembrane potential v (nondimensionalized so that $v=0$ and $v=1$ are the rest and peak voltages, respectively) and two gating variables f and s (mnemonics: f for the fast, s for the slow). The voltage changes in response to the ionic currents according to the relation,

$$\frac{dv}{dt}=-(J_{\mathrm{fast}}+J_{\mathrm{slow}}+J_{\mathrm{ung}}+J_{\mathrm{stim}}). \tag{3}$$

The fast inward current J_{fast} has the form,

$$J_{\mathrm{fast}}=-fQ(v)/\tau_{\mathrm{fast}}, \tag{4}$$

where τ_{fast} is a characteristic time for this current, the voltage dependence $Q(v)$ is given by

$$Q(v)=\begin{cases}(v-V_{\mathrm{crit}})(1-v) & \text{if } v>V_{\mathrm{crit}},\\ 0 & \text{if } v<V_{\mathrm{crit}},\end{cases} \tag{5}$$

and the gating variable f evolves according to

$$\frac{df}{dt}=[f_\infty(v)-f]/\tau_f(v). \tag{6}$$

The voltage-dependent functions on the right-hand side of Eq. (6) are step functions given by

$$\begin{aligned} f_\infty(v)&=0 \quad \text{and} \quad \tau_f(v)=\tau_{f\mathrm{close}} \quad \text{if } v>V_{f\mathrm{gate}},\\ f_\infty(v)&=1 \quad \text{and} \quad \tau_f(v)=\tau_{f\mathrm{open}} \quad \text{if } v<V_{f\mathrm{gate}}.\end{aligned} \tag{7}$$

Similarly, the slow inward current has the form,

$$J_{\mathrm{slow}}=-sS(v)/\tau_{\mathrm{slow}}, \tag{8}$$

where the sigmoid function $S(v)$ is given by

$$S(v)=\{1+\tanh[\kappa(v-V_{\mathrm{sig}})]\}/2, \tag{9}$$

and the gate variable s is governed by

$$\frac{ds}{dt}=[s_\infty(v)-s]/\tau_s(v), \tag{10}$$

with the right-hand side defined by

$$\begin{aligned} s_\infty(v)&=0 \quad \text{and} \quad \tau_s(v)=\tau_{s\mathrm{close}} \quad \text{if } v>V_{s\mathrm{gate}},\\ s_\infty(v)&=1 \quad \text{and} \quad \tau_s(v)=\tau_{s\mathrm{open}} \quad \text{if } v<V_{s\mathrm{gate}}.\end{aligned} \tag{11}$$

The ungated current has the form

$$J_{\mathrm{ung}}=P(v)/\tau_{\mathrm{ung}}, \tag{12}$$

where the piecewise-linear voltage dependence is given by

$$P(v)=\begin{cases}1 & \text{if } v>V_{\mathrm{out}},\\ v/V_{\mathrm{out}} & \text{if } v<V_{\mathrm{out}}.\end{cases} \tag{13}$$

[Our formula for $P(v)$ differs slightly from Fenton–Karma. By allowing the behavior of P to change at $V_{\mathrm{out}}\neq V_{\mathrm{crit}}$, we are able to make P continuous without changing the behavior of the model significantly.]

The stimulus current J_{stim} is an external current applied by the experimenter. Typically, $J_{\mathrm{stim}}(t)$ consists of a periodic train of brief pulses (with duration of 1 ms), each of approximately twice the strength required to excite fully recovered tissue. (In our units, the amplitude of each stimulus is $0.2\ \mathrm{ms}^{-1}$, so that the stimulus by itself, would raise the nondimensionless voltage by 0.2.) The currents J_{fast}, J_{slow}, and J_{ung} may be identified with sodium, calcium, and potassium currents, respectively. Table I lists the values of the parameters used by Fenton and Karma; we use these values in our calculations unless otherwise stated.

III. DERIVATION OF A SIMPLIFIED MAP FOR LARGE κ

In this section we consider periodic stimulation of the FK model. Let BCL denote the pacing interval, and let APD denote the time needed for the cell to repolarize after stimulation. We shall show that, with some approximation, the $(n+1)$st APD is a function of the previous APD and diastolic interval, i.e.,

$$\mathrm{APD}_{n+1}=G(\mathrm{APD}_n,\mathrm{DI}_n). \tag{14}$$

This formula has the same form as the empirical model developed in Refs. 16 and 17.

TABLE I. Parameters and their typical values for the Fenton–Karma three-current ionic model. (*) means that these parameters will be eliminated during the derivation of the map and the additional parameter DI_{th} will take their place.

Parameter	Value (ms)	Parameter	Value (dim′less)
(*) τ_{fast}	0.25	V_{crit}	0.13
τ_{slow}	127	V_{sig}	0.85
τ_{ung}	130	κ	10
(*) τ_{fclose}	10	V_{out}	0.1
(*) τ_{fopen}	18	V_{fgate}	V_{crit}
τ_{sclose}	1000	V_{sgate}	V_{crit}
τ_{sopen}	80		

If every stimulus produces an action potential, $DI_n = BCL - APD_n$, and (14) can be rewritten expressing APD_{n+1} as a function of APD_n and the parameter BCL as

$$APD_{n+1} = G(APD_n, BCL - APD_n). \tag{15}$$

More generally, if every Nth stimulus produces an action potential (an $N{:}1$ response), then (14) can be rewritten as

$$APD_{n+1} = G(APD_n, N*BCL - APD_n). \tag{16}$$

We shall call stimuli that actually produce an action potential *effective*. After an effective stimulus is applied, the tissue needs a certain time (DI_{th}) to be fully recovered. If the next stimulus is applied before DI_{th}, it will not produce an action potential; typically, one response occurs for every two stimuli (2:1 behavior).

A. Elimination of the fast current

Figure 1 shows the temporal evolution of the voltage v and the gating variables f and s according to numerical simulations of the FK model under periodic stimulation at $BCL = 700$ ms. It can be seen from the graphs that changes in the fast gating variable f occur much faster than changes in the voltage v and the gating variable s. Therefore, to simplify the model, we suppose that the fast current simply raises the voltage to the value $v = 1$ following an effective stimulus. This upstroke occurs so quickly that s does not changes appreciably, and after this upstroke J_{fast} vanishes until the next (effective) stimulus. In this approximation we need to consider only the motion in the (s,v) plane (see Fig. 2).

During the time while $V_{crit} < v < 1$ following the arrival of a stimulus at $t = t_{stim}$, Eq. (3) reduces to

$$\frac{dv}{dt} = \frac{s(t)}{\tau_{slow}} S(v) - \frac{1}{\tau_{ung}}, \tag{17}$$

with initial conditions

$$v(t_{stim}) = 1. \tag{18}$$

Assuming without loss of generality that $t_{stim} = 0$ the solution of (10) during this time is

$$s(t) = s(0) e^{-t/\tau_{sclose}}; \tag{19}$$

substitution of (19) into (17) yields,

$$\frac{dv}{dt} = \frac{s(0)}{\tau_{slow}} S(v) e^{-t/\tau_{sclose}} - \frac{1}{\tau_{ung}}. \tag{20}$$

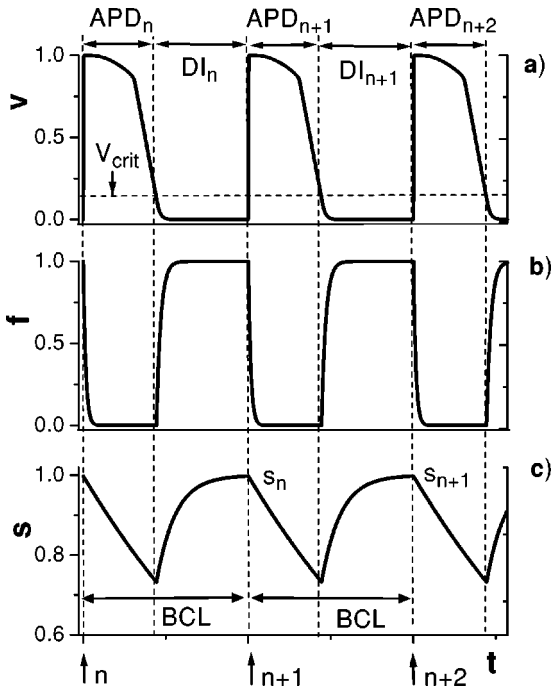

FIG. 1. Temporal evolution of (a) the voltage v, and gating variables (b) f, and (c) s, according to numerical simulations of the FK model with $BCL = 700$ ms. The arrows correspond to the times at which stimuli are applied.

The action potential produced by the stimulus has duration,

$$APD = t|_{v = V_{crit}} - t_{stim}, \tag{21}$$

obtained by solving Eq. (20) with the initial condition (18). Thus, the APD is a function of $s(t_{stim})$,

$$APD = \Phi[s(t_{stim})]. \tag{22}$$

In the context of periodic stimulation, as shown in Fig. 1, let s_n be the value of s at the time the $(n+1)$st effective

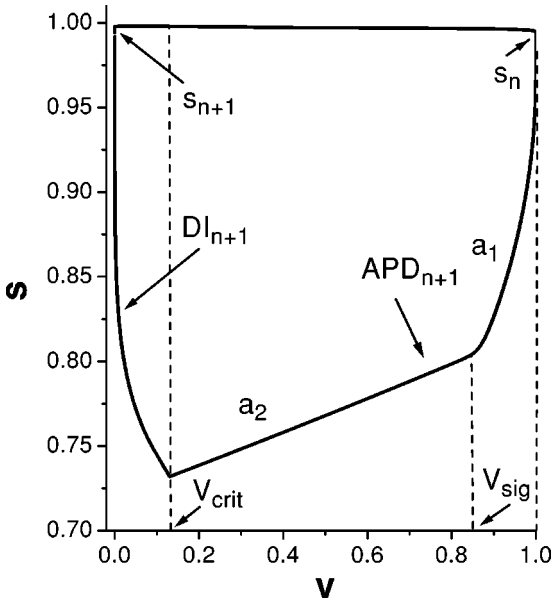

FIG. 2. Trajectory of the ODE's in the (s,v)-plane according to the FK model for the case $BCL = 700$ ms.

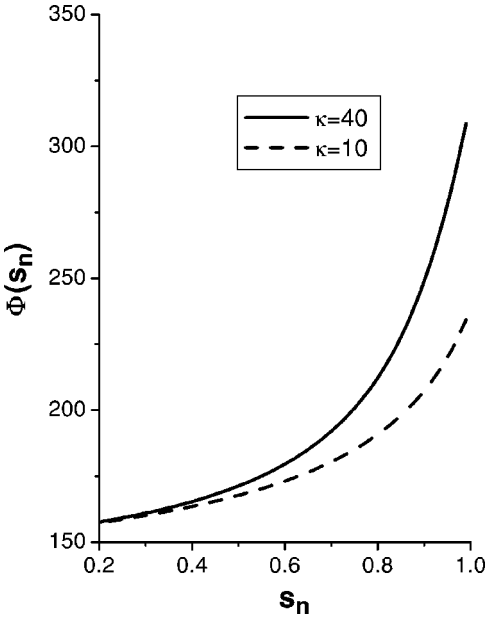

FIG. 3. Shape of the function $\Phi(s_n)$ from Eq. (23) according to the FK model for two values of the parameter κ.

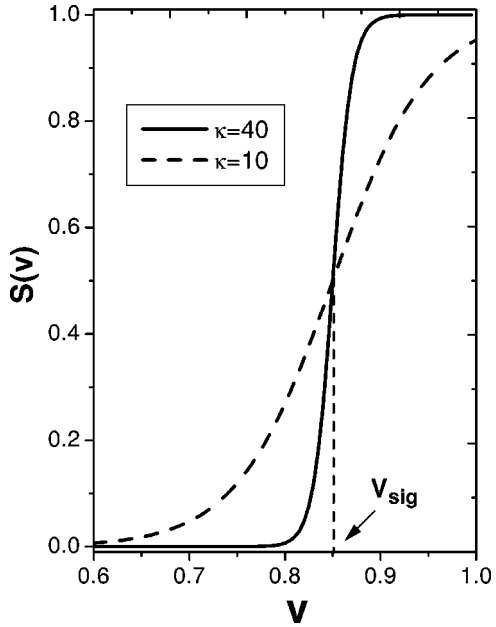

FIG. 4. Form of the function $S(v)$ given by (9) for two values of the parameter κ.

stimulus arrives, and let APD_{n+1} be the duration of the $(n+1)$st action potential. Rewriting (22) in this notation we obtain

$$\mathrm{APD}_{n+1}=\Phi(s_n). \tag{23}$$

In general, there is no explicit formula for the function Φ. Numerical computations of this function are graphed in Fig. 3 for two different values of the parameter κ. (In Sec. III C we shall derive an approximate formula for Φ under the hypothesis that κ is large.)

We claim that

$$s_n=1-(1-s_{n-1}^*)e^{-DI_n/\tau_{\mathrm{sopen}}}, \tag{24}$$

where

$$s_{n-1}^*=s_{n-1}e^{-\mathrm{APD}_n/\tau_{\mathrm{sclose}}}. \tag{25}$$

Indeed, (25) results from solving (10) from the arrival of the nth stimulus until $v=V_{\mathrm{crit}}$, and (24) results from continuing the solution of (10) from the time when $v=V_{\mathrm{crit}}$ until the next (effective) stimulus. Replacing n by $(n-1)$ in (23) and inverting the function Φ, we may rewrite (25) as

$$s_{n-1}^*=\Phi^{-1}(\mathrm{APD}_n)e^{-\mathrm{APD}_n/\tau_{\mathrm{sclose}}}. \tag{26}$$

Substituting (24) and (26) into (23), we obtain (14) with

$$G(\mathrm{APD}_n,\mathrm{DI}_n)=\Phi(1-[1-\Phi^{-1}(\mathrm{APD}_n)e^{-\mathrm{APD}_n/\tau_{\mathrm{sclose}}}]\times e^{-\mathrm{DI}_n/\tau_{\mathrm{sopen}}}). \tag{27}$$

Thus, expression (27) represents our main result, i.e., the map derived on the basis of the FK model. This map has the same form as the one obtained empirically by Otani and Gilmour in Ref. 16 using a memory model.

B. Comparison with the two-current ionic model

As an aside, we note that a restitution map of the simpler form (1) was derived by Karma.[14] As elaborated in Ref. 15, one obtains

$$G(\mathrm{DI}_n)=\tau_{\mathrm{close}}\ln\left(\frac{1-(1-s_{\min})e^{-\mathrm{DI}_n/\tau_{\mathrm{sopen}}}}{s_{\min}}\right), \tag{28}$$

where $s_{\min}$ is a constant. Comparing (28) with (27) we can see that the simplification

$$\Phi^{-1}(\mathrm{APD}_n)e^{-\mathrm{APD}_n/\tau_{\mathrm{sclose}}}=s_{\min} \tag{29}$$

occurs. Thus, (28) gives a restitution map of the familiar form that depends on the previous DI but not the previous APD. Also note that while Φ in Fig. 3 obtained from the three-current model is convex *upward*, (28) is convex *downward*. Therefore, there is not any parameter region in which the three-current model reduces to the two-current model.

C. Approximation for large κ

As noted above, (20) cannot be solved analytically with $S(v)$ given by (9), preventing us from obtaining an explicit formula for Φ in general. In Fig. 4 we have graphed $S(v)$ for two values of the parameter κ, the original value chosen by Fenton and Karma ($\kappa=10$) and a large value $\kappa=40$. In this subsection, assuming that κ is large, we approximate $S(v)$ by a step function,

$$S(v)=\begin{cases}1 & \text{if } v>V_{\mathrm{sig}},\\ 0 & \text{if } v<V_{\mathrm{sig}},\end{cases} \tag{30}$$

and then solve (20) analytically. (In Sec. IV C below we will consider moderate κ.)

Following the arrival of the $(n+1)$st effective stimulus Eq. (20) becomes, using approximation (30),

$$\frac{dv}{dt}=\begin{cases}\dfrac{s_n}{\tau_{\rm slow}}e^{-t/\tau_{\rm sclose}}-\dfrac{1}{\tau_{\rm ung}} & \text{if } V_{\rm sig}<v<1,\\ -\dfrac{1}{\tau_{\rm ung}} & \text{if } V_{\rm crit}<v<V_{\rm sig},\end{cases} \tag{31}$$

which may be solved analytically. We decompose the APD_{n+1} given by Eq. (21) into the sum of two contributions coming from the two alternatives in (31),

$$\mathrm{APD}_{n+1}\equiv\Phi(s_n)=a_1+a_2, \tag{32}$$

where

$$a_1=t|_{v=V_{\rm sig}}-t|_{v=1},\quad a_2=t|_{v=V_{\rm crit}}-t|_{v=V_{\rm sig}}. \tag{33}$$

Solving (31), we see that a_1 and a_2 satisfy

$$\frac{s_n\tau_{\rm sclose}}{\tau_{\rm slow}}(e^{-a_1/\tau_{\rm sclose}}-1)+\frac{a_1}{\tau_{\rm ung}}-1+V_{\rm sig}=0, \tag{34}$$

$$a_2=\tau_{\rm ung}(V_{\rm sig}-V_{\rm crit}). \tag{35}$$

A formula for the inverse function Φ^{-1} of (23) can be obtained without further approximation. By (32) and (35),

$$a_1=\mathrm{APD}_{n+1}-\tau_{\rm ung}(V_{\rm sig}-V_{\rm crit}); \tag{36}$$

substituting this into (34), replacing n by $n-1$ and solving for s_{n-1} we obtain

$$s_{n-1}\equiv\Phi^{-1}(\mathrm{APD}_n)=\frac{\dfrac{\mathrm{APD}_n}{\tau_{\rm ung}}-(1-V_{\rm crit})}{1-\exp\{[-\mathrm{APD}_n+\tau_{\rm ung}(V_{\rm sig}-V_{\rm crit})]/\tau_{\rm sclose}\}}\,\frac{\tau_{\rm slow}}{\tau_{\rm sclose}}. \tag{37}$$

To derive a formula for the function Φ itself, we need to make an additional approximation based on the fact that $\tau_{\rm sclose}$, which appears in the exponent in (37), is much larger than any of the other quantities in the model. Thus, we use a power series expansion of $\exp[-z]\approx 1-z+z^2/2+O(z^3)$, where $z\equiv a_1/\tau_{\rm sclose}\ll 1$, which allows us to rewrite (37) as a quadratic equation for the APD_{n+1} and obtain

$$\mathrm{APD}_{n+1}=\Phi(s_n)=\tau_{\rm sclose}\left[C_1-\frac{\tau_{\rm slow}}{\tau_{\rm ung}s_n}+\sqrt{1-\frac{C_2}{s_n}+\left(\frac{\tau_{\rm slow}}{\tau_{\rm ung}s_n}\right)^2}\right], \tag{38}$$

where

$$C_1=1+\frac{\tau_{\rm ung}}{\tau_{\rm sclose}}(V_{\rm sig}-V_{\rm crit}),$$

$$C_2=2\tau_{\rm slow}\left[\frac{1}{\tau_{\rm ung}}+\frac{(V_{\rm sig}-1)}{\tau_{\rm sclose}}\right]. \tag{39}$$

Substitution of expressions (37)–(39) into (27) gives the explicit form of the function G for the case of large κ.

D. Comparison of the mapping with numerical simulations of the ODE's

For a fixed value of BCL, consider iteration of (16) with G given by (27), where Φ and Φ^{-1} are given by (38) and (37), respectively. The function G is presented in Fig. 5 (thick solid lines) for BCL = 200 ms and $N=1$ and 2. The intersection of the graph of $G(\mathrm{APD}_n, N*BCL-\mathrm{APD}_n)$ with the diagonal $\mathrm{APD}_{n+1}=\mathrm{APD}_n$ (solid line) gives the fixed points of the map. The dashed line,

$$\mathrm{APD}_n=BCL-\mathrm{DI}_{\rm th} \tag{40}$$

indicates when the response switches from $N=1$ to $N=2$ response patterns, as we discuss below.

In Fig. 6 we show bifurcation diagrams obtained from (16) and from numerical simulation of the ODE's with $\kappa=40$. For the ODE's, we start from a very long BCL, apply at least 100 stimuli (in order to eliminate transients), and record the APD resulting from the last; then we decrease the BCL by 2 ms and repeat the procedure. We continue this procedure down to a small value of BCL. As shown in the Fig. 6, at sufficiently small BCL, the system jumps from an $N=1$ response to an $N=2$ response (denoted by th_1). After this downsweep of BCL, we start from a short BCL and increase BCL on each step obtaining an upsweep. The jump from $N=2$ response to $N=1$ response occurs at a different

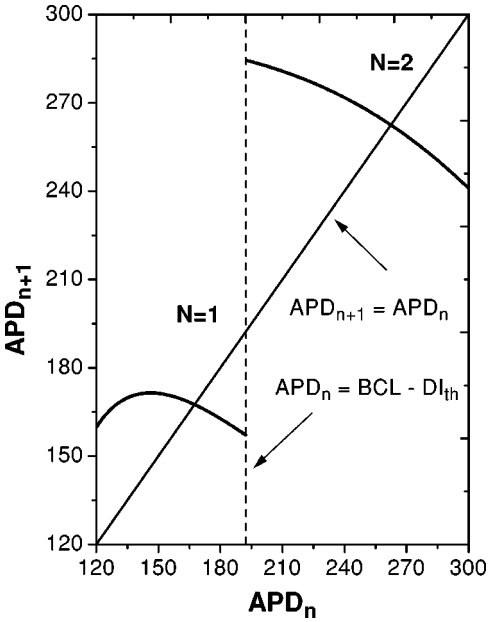

FIG. 5. Graph of $G(\mathrm{APD}_n, N*BCL-\mathrm{APD}_n)$ for the case of large κ, for $BCL=200$ ms, $\mathrm{DI}_{\rm th}=7$ ms, $N=1$ and 2. Values of other parameters are given in Table I.

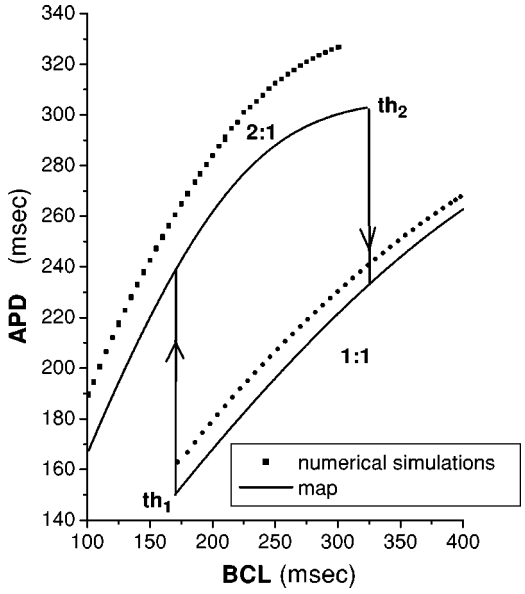

FIG. 6. Bifurcation diagrams obtained from numerical simulations of the FK model (squares) and iterated map for $DI_{th}=20$ ms, $\kappa=40$.

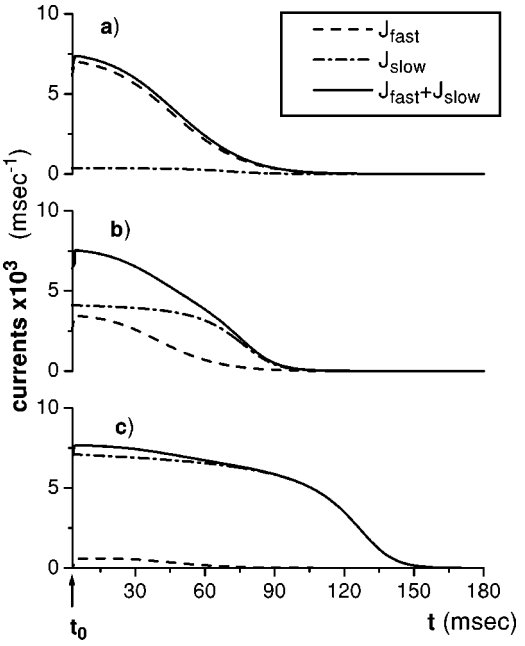

FIG. 7. Time evolution of inward (fast and slow) currents and their sum for the different initial values of the slow current: (a) $s_n=0.05$; (b) $s_n=0.55$; (c) $s_n=0.95$.

point (th_2) than in the downsweep. Thus, an hysteresis loop is observed by changing the BCL from short to long values and back.[18] For some region of BCL, both stable 1:1 and 2:1 solutions exist. The existence of such bistability regions in forced piecewise-linear Fitzhugh–Nagumo-type systems for some parameter values was proved mathematically in Refs. 19 and 20.

The points (BCL,APD) in Fig. 6 computed from the map represent fixed points of (16). For a point (BCL,APD) on the bifurcation diagram corresponding to an $N=1$ response,

$$BCL-\mathrm{APD}>\mathrm{DI_{th}}; \tag{41}$$

otherwise there would not be sufficient time for the cell to respond to the next stimulus. Similarly, for an $N=2$ response,

$$BCL-\mathrm{APD}<\mathrm{DI_{th}}. \tag{42}$$

Since the parameter DI_{th} does not occur explicitly in the FK model (it replaces the fast current), we have to introduce it in the map by hand. Following (41), we choose the value of DI_{th} in such a way that the jump from 1:1 to 2:1 solutions during the map iteration takes place at the same point (th_1) as happens according to numerical simulations of the FK model.

One can see from the graphs presented in the Fig. 6 that there is good qualitative agreement between the bifurcation diagrams obtained from the numerical simulation of the original ODE's and from the map iteration (in particular, both bifurcation diagrams exhibit bistability and have the same qualitative shape). Even though the quantitative agreement is not perfect, this simplification still contains most of the important physiological effects and should be useful for explaining experimental results through adjustment of parameters. In Sec. IV, we will explain the reason for the discrepancy between the predictions of the map and the ODE's and will improve the map to achieve better quantitative agreement.

IV. THREE REFINEMENTS TO THE MAP

In this section we discuss three refinements that achieve better quantitative agreement between the map and the model. The first refinement is based on the fact that the fast sodium current is strongly coupled with the other currents in the FK model and so the process of eliminating the fast current should be re-examined. The second refinement deals with an additional increase of the APD that occurs for the case of 2:1 behavior due to the effect of subthreshold response (see, for instance, Refs. 12, 21, and 22). In the third refinement we derive a map for the case of moderate κ, because this parameter regime corresponds more closely to the value used in the original FK model.

A. Elimination of the fast current re-examined

In deriving a simplified map from the FK model, we dropped the term that describes the fast sodium current J_{fast} from Eq. (3), based on the fact that changes in the gate variable f occur much faster than changes in the voltage v and gating variable s. Actually, the fast gating variable f does decay to zero quickly (see Fig. 1), but surprisingly the fast current J_{fast} may not decay as quickly. In Fig. 7, the time evolution of J_{slow}, J_{fast}, and their sum (based on numerical simulations of the FK model) is presented for different initial values of the slow current (s_n) starting a few msec after the stimulus arrived (let us call this time as t_0). Note that the value of the fast current should already be negligible (because $\tau_{fast}\ll t_0$) according to our previous assumption. However, as can be seen from Fig. 7, the value of the fast current can still be significant depending on initial value of the slow

current s_n. This occurs for the following reason: if J_{slow} is suppressed, the voltage following stimulation falls faster than otherwise, and as a result the voltage-dependent function $Q(v)$ in (4) is larger than otherwise, partially compensating for the decay of f. Indeed, although the values of J_{slow} and J_{fast} are different in the three cases in Fig. 7, their sum has nearly the same initial value in all three cases, which is approximately equal to J_{ung},

$$J_{\text{slow}}+J_{\text{fast}}\simeq J_{\text{ung}}. \tag{43}$$

This fact is a feature of the FK model (even though it is not physiological), and we have to take it into account in order to achieve a full correspondence between the map and the model. Thus, we propose the following procedure to eliminate the fast current: we assume that instead of complete elimination of the fast current ($J_{\text{fast}}=0$) we keep part of it, which can be significant when $v\sim 1$ and the value of the slow current is small. Following this logic, the expression for the fast current that we retain can be found from Eqs. (4)–(7) and is taken as

$$J_{\text{fast}}=-\frac{f(t_{\text{stim}})Q(v)}{\tau_{\text{fast}}}e^{-t/\tau_{f\text{close}}}\simeq-\frac{f(t_{\text{stim}})\tilde{Q}(v,t)}{\tau_{\text{fast}}}. \tag{44}$$

In order to determine $f(t_{\text{stim}})$, consider Eq. (43) at the moment t_0 using Eqs. (4), (8), and (12),

$$\frac{Q_0 f(t_0)}{\tau_{\text{fast}}}+\frac{S_0 s(t_0)}{\tau_{\text{slow}}}-\frac{1}{\tau_{\text{ung}}}\simeq 0, \tag{45}$$

so that

$$f(t_0)=\left[\frac{1}{\tau_{\text{ung}}}-\frac{S_0 s(t_0)}{\tau_{\text{slow}}}\right]\frac{\tau_{\text{fast}}}{Q_0}, \tag{46}$$

where Q_0 and S_0 are values of functions $\tilde{Q}(v,t)$ and $S(v)$ at time t_0 ($S_0\simeq 1$ because $v\sim 1$). Here we used the approximation: $\exp[-t_0/\tau_{s\text{close}}]$, $\exp[-t_0/\tau_{f\text{close}}]\approx 1$, since $t_0 \ll \tau_{s\text{close}}, \tau_{f\text{close}}$. Equation (3) can be rewritten using (44) and (46) and assuming that $t_0\simeq t_{\text{stim}}$, so that

$$\frac{dv}{dt}=\frac{s_n}{\tau_{\text{slow}}}S(v)e^{-t/\tau_{s\text{close}}}-\frac{1}{\tau(v,s_n)}, \tag{47}$$

where

$$\frac{1}{\tau(v,s_n)}=\frac{\tilde{Q}(v,t)}{Q_0}\left(\frac{1}{\tau_{\text{ung}}}-\frac{s_n}{\tau_{\text{slow}}}\right)-\frac{1}{\tau_{\text{ung}}}. \tag{48}$$

Here, as before, s_n is the value of $s(t_{\text{stim}})$ at the arrival time of the $(n+1)$st stimulus. Note that the only difference between Eqs. (20) and (47) is that the parameter τ_{ung} from the first equation becomes a variable $\tau(v,s_n)$ in the latter one.

The presence of v-dependent functions $\tau(v,s_n)$ in Eq. (47) makes it impossible to solve analytically as was done in Sec. III for the simplified case. Hence, we must use other simplifications. Our analysis shows that the function $\tilde{Q}(v,t)$ does not play a crucial role in determining the APD; it only prevents the fast current from decaying when there is not enough slow current. To avoid difficulties coming from this term, we assume that $\tilde{Q}(v,t)/Q_0\equiv\zeta_1=\text{const}$, and write down empirically the total APD_{n+1} calculated from Eq. (47) as

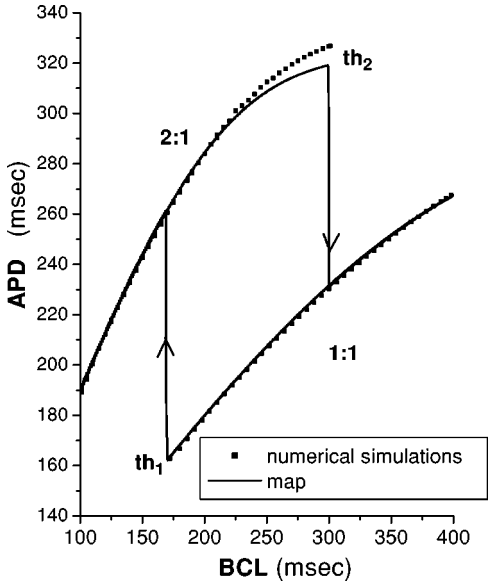

FIG. 8. Bifurcation diagrams, similar to ones presented in the Fig. 6, for the case when two refinements are taken into account during the map derivation with $\nu_1=0.8, \nu_2=1.4,$ and $\zeta_1=0.2$.

$$\text{APD}_{n+1}=\nu_1 a_1+\nu_2 a_2+A_0, \tag{49}$$

where ν_1 and ν_2 are constants chosen by hand for each κ, based on comparison with results of numerical simulations, and the meaning of the term A_0 will be explained in the next section. We find that ν_1 and ν_2 do not change if other parameters are changed.

Thus, the results of our first refinement is that we have to solve the equation

$$\frac{dv}{dt}=\frac{s_n}{\tau_{\text{slow}}}S(v)e^{-t/\tau_{s\text{close}}}+\zeta_1\left(\frac{1}{\tau_{\text{ung}}}-\frac{s_n}{\tau_{\text{slow}}}\right)-\frac{1}{\tau_{\text{ung}}} \tag{50}$$

instead of Eqs. (20) and use formula (49) to determine the APD_{n+1}.

B. Effect of subthreshold response: Comparison with results of numerical simulations of the FK model

We make a second refinement based on the fact that, following an ineffective stimulus, the APD is increased due to the subthreshold effect. This effect was described in Refs. 21 and 22, where the response of a modified Beeler–Reuter model to periodic stimulation by rectangular stimuli was studied. Later, the subthreshold response was mentioned in Ref. 12 where transitions from a 1:1 to a 2:1 rhythm in periodically driven single ventricular cells were analyzed based on the LR1 model. When the 2:1 behavior occurs, only the first stimulus is effective and produces an action potential, and the second stimulus does not because it is applied before the cell is fully recovered. However, the effect of the second stimulus on the APD is to prolong it due to the stimulus artifact. We have found from numerical simulations that this additional increase of the APD for the case of 2:1 be-

havior is approximately the same for any value of the BCL. We take this effect into account adding constant A_0 to the expression (49),

$$A_0=\begin{cases}27 \text{ ms}, & N=2,\\ 0, & N=1.\end{cases} \tag{51}$$

In Fig. 8, bifurcation diagrams similar to the ones from Fig. 6 are presented. Here, the two refinements described above are taken into account. One can see from the graphs that there is good agreement, both qualitative and quantitative, between these bifurcation diagrams: the slope of the curves is similar and jump points th_1 and th_2 are nearly equal.

C. Derivation of the map for moderate κ

As we have mentioned, we can only find an explicit formula for the function G constituting our map (14) for the case of large κ. In general, the shape of this function (which is determined by the function Φ) depends on the value of κ (see Fig. 3). Typically, the value of κ used in the literature (see, for instance, Ref. 7) is not so large ($\kappa\simeq 10$). Here we present a map derived for the case of moderate κ. For this purpose we approximate $S(v)$ by a piecewise linear function,

$$S(v)=\begin{cases}\alpha v+\beta & \text{if } v>V_0,\\ 0 & \text{if } v<V_0,\end{cases} \tag{52}$$

where

$$\alpha=\frac{1}{1-V_0}, \quad \beta=-\frac{V_0}{1-V_0}, \tag{53}$$

and V_0 is chosen by hand depending on value of the κ in order to achieve a better fit with the original shape of the function $S(v)$ (for instance, $V_0=0.7$ for $\kappa=10$).

Following the arrival of the $(n+1)$st effective stimulus, Eq. (47) becomes, according to approximation (52),

$$\frac{dv}{dt}=\begin{cases}(\alpha v+\beta)\dfrac{s_n}{\tau_{\text{slow}}}e^{-t/\tau_{\text{sclose}}}-\dfrac{1}{\tau(s_n)} & \text{if } V_0<v<1,\\ -\dfrac{1}{\tau_{\text{ung}}} & \text{if } V_{\text{crit}}<v<V_0,\end{cases} \tag{54}$$

which may be solved analytically. Similar to the case of large κ, we decompose the APD_{n+1} given by Eq. (21) into the sum of two contributions coming from the two expressions in (54), so that Eq. (32) [which is now written as Eq. (49)] is valid with

$$a_1=t|_{v=V_0}-t|_{v=1}, \quad a_2=t|_{v=V_{\text{crit}}}-t|_{v=V_0}. \tag{55}$$

Solving (54), we can find expressions to determine a_1 and a_2,

$$F(a_1)\equiv e^{-g}C-\frac{\beta}{\alpha}+\frac{\tau_{\text{sclose}}}{\tau(s_n)}\text{Ei}[g]e^{-g}-V_0=0, \tag{56}$$

$$a_2=\tau_{\text{ung}}(V_0-V_{\text{crit}}), \tag{57}$$

where C is the integral constant defined from the initial condition (18),

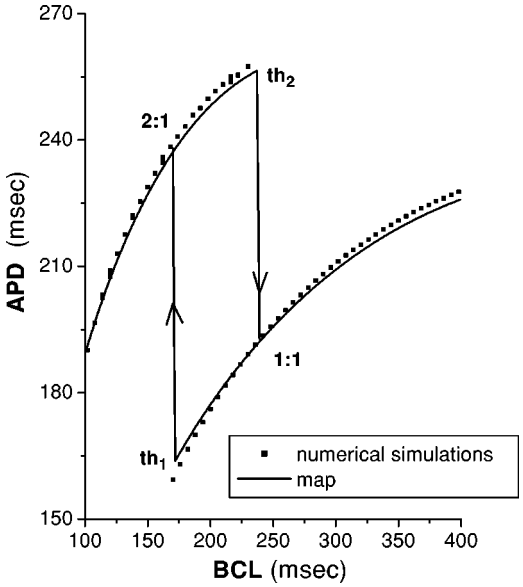

FIG. 9. Bifurcation diagrams obtained from the numerical simulations of the FK model and iteration of the map with $\kappa=10$, $\text{DI}_{\text{th}}=10$ ms, $\nu_1=1.35$, $\nu_2=1$, and $\zeta_1=0.35$.

$$C=e^{g_0}\left[1+\frac{\beta}{\alpha}-\frac{\tau_{\text{sclose}}}{\tau(s_n)}\text{Ei}[g_0]e^{-g_0}\right], \tag{58}$$

$\text{Ei}[z]$ is the exponential integral function,

$$\text{Ei}[z]=\int_{-z}^{\infty}\frac{e^{-t}}{t}dt, \tag{59}$$

and

$$g=g_0e^{-a_1/\tau_{\text{sclose}}}, \quad g_0=\alpha s_n\frac{\tau_{\text{sclose}}}{\tau_{\text{slow}}}. \tag{60}$$

Note that a_1 is now an implicit function of s_n and can be found only numerically, so that both the functions Φ and Φ^{-1}, and thus the function G representing the total map (27), are implicit.

Figure 9 shows bifurcation diagrams for the case of moderate κ obtained from numerical simulations of the FK model and iteration of the map. We see that these results are in good agreement. Comparing Figs. 8 and 9, we see a small difference between the bifurcation diagrams for different values of the parameter κ; for the case of large κ the value of the APD is larger when the 2:1 behavior takes place, and the range of the BCL where bistability occurs is wider. For instance, the jump from the upper to the lower branch (th_2) for moderate κ occurs at $BCL\sim 250$ ms with $\text{APD}\sim 255$ ms, and for large κ at $BCL\sim 300$ ms with $\text{APD}\sim 320$ ms, respectively. The slopes of the branches are also slightly different for both cases.

V. CONCLUSIONS

In this paper, we apply asymptotic analysis to derive a map from the Fenton–Karma ODE's that predict the response of a cardiac cell to periodic external stimulation. The map has the general form $\text{APD}_{n+1}=G(\text{DI}_n,\text{APD}_n)$, and thus it contains some amount of memory due to its depen-

dence on two variables. Our work places the empirical proposal of Otani and Gilmore,[16] who put forth a map of the same general form, on a rigorous mathematical foundation (although the specific function G is different in their proposal). We find that the agreement between the predictions of the Fenton–Karma ODE's and the map are in good agreement when the model parameter κ is large, and we describe various refinements to the map, including one that extends its useful range to moderate values of κ.

We believe the simplified map will be helpful in fitting the FK model to experimental data. One may employ a two-stage procedure: first choosing parameters in the map to obtain a rough fit to the data, and then refining the fit using numerical simulations of the ODE's. Application of this procedure to the experiments[18] will be published elsewhere. In that paper we will also document a property of the model not derived in this paper, i.e., the model displays rate-dependent restitution, and hence the dynamic and $S1-S2$ restitution curves are different.

ACKNOWLEDGMENT

We gratefully acknowledge the support of the NSF under Grant No. PHY-9982860.

[1] G. Beeler and H. Reuter, "Reconstruction of the action potential of ventricular myocardial fibres," J. Physiol. (London) **268**, 177 (1977).
[2] C. Luo and Y. Rudy, "A model of the ventricle cardiac action potential: Depolarization, repolarization, and their interaction," Circ. Res. **68**, 1501 (1991).
[3] C. Luo and Y. Rudy, "A dynamical model of the cardiac ventricular action potential. 1. Stimulations of ionic currents and concentration changes," Circ. Res. **74**, 1071 (1994).
[4] M. Courtemanche, R.J. Ramirez, and S. Nattel, "Ionic mechanisms underlying human atrial action potential properties: Insights from a mathematical model," Am. J. Physiol. **275**, H301 (1998).
[5] R.R. Aliev and A.V. Panfilov, "A simple two-variable model of cardiac excitation," Chaos, Solitons Fractals **7**, 293 (1996).
[6] G. Duckett and D. Barkley, "Modeling the dynamics of cardiac action potential," Phys. Rev. Lett. **85**, 884 (2000).
[7] F. Fenton and A. Karma, "Vortex dynamics in three-dimensional continuous myocardium with fiber rotation: Filament instability and fibrillation," Chaos **8**, 20 (1998).
[8] S.H. Strogatz, *Nonlinear Dynamics and Chaos* (Perseus, Reading, MA, 1994).
[9] G.R. Mines, "On dynamic equilibrium in the heart," J. Physiol. (London) **48**, 349 (1913).
[10] J.B. Nolasco and R.W. Dahlen, "A graphic method for the study of alternation in cardiac action potential," J. Appl. Physiol. **25**, 191 (1968).
[11] M. Guevara, G. Ward, A. Shrier, and L. Glass, "Electrical alternans and period doubling bifurcations," *Computers in Cardiology* (IEEE Computer Society, Silver Spring, MD, 1984), p. 167.
[12] A.R. Yehia, D. Jeandupeux, F. Alonso, and M.R. Guevara, "Hysteresis and bistability in the direct transition 1:1 to 2:1 rhythm in periodically driven single ventricular cells," Chaos **9**, 916 (1999).
[13] D.R. Chialvo, D.C. Michaels, and J. Jalife, "Supernormal excitability as a mechanism of chaotic dynamics of activation in cardiac Purkinje fiber," Circ. Res. **66**, 525 (1990).
[14] A. Karma, "Electrical alternans and spiral wave breakup in cardiac tissue," Chaos **4**, 461 (1994).
[15] C.C. Mitchell and D.G. Schaeffer, "A two-current model for the dynamics of cardiac membrane," Bull. Math. Bio. (submitted).
[16] N.F. Otani and R.F. Gilmour, Jr., "Memory models for the electrical properties of local cardiac systems," J. Theor. Biol. **187**, 409 (1997).
[17] R.F. Gilmour, Jr., N.F. Otani, and M.M. Watanabe, "Memory and complex dynamics in cardiac Purkinje fiber," Am. J. Physiol. **272**, H1826 (1997).
[18] G.M. Hall, S. Bahar, and D.J. Gauthier, "Prevalence of rate-dependent behaviors in cardiac muscle," Phys. Rev. Lett. **82**, 2995 (1999).
[19] H.G. Othmer and M. Xie, "Subharmonic resonance and chaos in forced excitable systems," J. Math. Biol. **39**, 139 (1999).
[20] M. Xie, H.G. Othmer, and M.M. Watanabe, "Resonance in excitable systems under step-function forcing. II. Subharmonic solutions and persistence," Physica D **98**, 75 (1996).
[21] A. Vinet and F.A. Roberge, "Excitability and repolarization in an ionic model of the cardiac cell membrane," J. Theor. Biol. **170**, 183 (1994).
[22] A. Vinet and F.A. Roberge, "Analysis of an iterative difference equation model of the cardiac cell membrane," J. Theor. Biol. **170**, 201 (1994).